frontiers | Frontiers in Nutrition

TYPE Original Research
PUBLISHED 09 January 2023
DOI 10.3389/fnut.2022.1075296

OPEN ACCESS

EDITED BY
Mahmood Alizadeh Sani,
Tehran University of Medical Sciences, Iran

REVIEWED BY
Lingshan Gong,
University of North Texas, United States
Tao Le,
Chongqing Normal University, China
Xi Yu,
Macau University of Science and Technology, Macao SAR, China

*CORRESPONDENCE
Chongning Li
lcn7882342@qq.com
Zhiliang Jiang
zljiang@gxnu.edu.cn

SPECIALTY SECTION
This article was submitted to Food Chemistry, a section of the journal Frontiers in Nutrition

RECEIVED 11 November 2022
ACCEPTED 21 December 2022
PUBLISHED 09 January 2023

CITATION
Li J, Shu Y, Li C and Jiang Z (2023) Highly catalytic nanoenzyme of covalent organic framework loaded starch- surface-enhanced Raman scattering/absorption bi-mode peptide as biosensor for ultratrace determination of cadmium. *Front. Nutr.* 9:1075296. doi: 10.3389/fnut.2022.1075296

Highly catalytic nanoenzyme of covalent organic framework loaded starch-surface-enhanced Raman scattering/absorption bi-mode peptide as biosensor for ultratrace determination of cadmium

Jingjing Li[1,2], Yiyi Shu[1,2], Chongning Li[1,2]* and Zhiliang Jiang[1,2]*

[1]School of Public Health, Guilin Medical University, Guilin, China, [2]Guangxi Key Laboratory of Environmental Pollution Control Theory and Technology, Guilin, China

High affinity peptides (PTs) have been used in nanoanalysis, but there are no reports which combine PTs with a liquid crystal (LC) covalent organic framework (COF) supported soluble starch (SS) catalytic amplification system as a biosensor recognition element. In this study, a new, highly sensitive and selective bi-mode molecular biosensor has been developed for the determination of cadmium ion (Cd^{2+}). Specifically, a highly catalytic and stable COF supported SS nanosol catalyst was fabricated such that a nanocatalytic indicator reaction system for $HAuCl_4$-sodium formate was established based on surface-enhanced Raman scattering (SERS). The Au nanoparticles produced exhibited a surface plasmon resonance (SPR) absorption peak at 535 nm and a SERS peak at 1,615 cm^{-1}. Combining the nanocatalytic amplification indicator system with the specific PTs reaction permitted a sensitive and selective SERS/absorption bi-mode platform to be developed for the determination of cadmium in rice. The linear range for SERS determination was 0.025–0.95 nmol/L and the detection limit (DL) was 0.012 nmol/L.

KEYWORDS

Cd^{2+}, peptides, COF loaded-SS catalysis, SERS, gold nanoparticle, indicator reaction

1. Introduction

Peptides (PTs) which are widely available and of relatively low cost have good biocompatibility and water solubility properties. They also have a high affinity for many metal ions and have become excellent receptors for use in methodologies which

exploit molecular recognition chemistry. Among them, absorption, fluorescence and electrochemical methods are used frequently in chemical analysis (1, 2). Zhuang et al. (3) reported a peptide fluorescent probe TP-2 (TPE-TrP-Pro-GlN-His-Glu-NH_2), which utilized an aggregation-induced emission effect and afforded high selectivity in the determination of Hg^{2+}, the detection limit (DL) being 41 nM. Yu et al. (4) immobilized an antibody against C-peptide onto TRF microspheres in a directional manner, thus fully exposing the antigen binding site, to determine C-peptide in human serum with a DL of 0.005 ng/mL. Furthermore, DNA and metal ions can be also determined by using PT-based sensors (5-7). However, to the best of our knowledge there are no reports on the use of a PT sensor for the determination of Cadmium ion (Cd^{2+}) based on quantitative surface-enhanced Raman scattering (SERS) analysis, whereby a covalent organic framework (COF) loaded soluble starch (SS) facilitates nanocatalytic amplification.

SERS is a versatile analytical technique in the biosciences and affords high sensitivity, rapid and non-destructive analysis and multiple measurement capability (8-10). Based on the competitive binding between Au nanoparticles and RKGSGRRLVKC (11 peptide) and CALNN (5 peptide), SERS has been used to determine heparin (11), the analytical range being 0.2–2.4 μg/mL with a DL of 0.042 μg/mL. Liang et al. (12) studied the combination of catalytic graphene oxide nanoribbons (GONR) and human chorionic gonadotropin (hCG) polypeptide as a novel biosensor and established a new GONR-catalyzed RRS/absorption method to determine hCG with a DL of 70 pg/mL.

The COFs are a class of crystalline porous organic polymers that use small organic monomers as building blocks that are connected by covalent bonds. The pore structures, the strong light absorption ability and the tunable structures have attracted much interest recently (13, 14). In fact, COFs have been used as a multifunctional platform for gas adsorption and separation, sensing, and proton conduction, energy storage and heterogeneous catalysis (15, 16). The synthesis of COFs can be carried out using a variety of procedures including those based on solvothermal, ionothermal, and microwave energy (17). Most of these procedures, however, require relatively hazardous conditions and relatively long COF package crystallization times. As attractive synthesis routes, mechanical chemical polishing and hydrothermal treatment at room temperature are facilitating the extensive application and preparation of the COF package (18) as evidenced by recent studies (19-21) in optics, chemistry and electronics. Also, SERS has been applied to the determination of metal ions, based on the use of COF materials (22, 23). To improve the performance of the COFs, the doping of metal nanoparticles into the COFs is simple and effective strategy. In this approach, the number of free electrons on the surface of the COFs is increased, thereby facilitating the transfer of redox electrons and promoting the intended reaction (24). Starch is a common natural polydextrose (25, 26). In natural starch, amylose, which is soluble, accounts for 20∼26% of the total content, the remainder consisting of amylopectin. Oyamada et al. reported (26) that three amylose alkyl carbamate esters, namely, amylose triester (n-butylcarbamate), amylose triester (ethyl carbamate), and amylose triester (hexyl carbamate) in tetrahydrofuran form different liquid crystal (LC) phases that exhibit lyotropic liquid crystallinity. However, the thermotropic LC properties are rarely reported for amylose. Amylose has been used as an end sealer for metal and bimetal nanoparticles. Balasurya et al. (27) developed a novel core-shell Fe@Ag-starch nanosphere phenylalanine conjugate, and determined trace levels (1.84 nmol/L) of Hg^{2+} by absorption (Abs) spectrophotometry. Sapyen et al. (28) used SS-capped AgNPs in combination with a colorimetric method to determine trace levels (48 μg/L) of Cr (VI). Though starch as a natural polymer is cheap and may be used in nanoanalysis, little attention has been given to the stabilization of starch nanoparticles in catalytic reactions.

Cadmium ion is a toxic heavy metal and may be removed from polluted and contaminated waters by ion exchange, electrolysis, chemical precipitation, bioremediation or adsorption (29). However, chemical precipitation would result in sedimentation, which could then cause secondary pollution (30). Ion-exchange and electrolysis methods, while more efficient, have much higher maintenance costs (31). Therefore, to establish a highly sensitive and selective method for the determination of trace levels of Cd^{2+} is of great significance. Traditional analytical methods for the determination of Cd^{2+} include electrochemical, colorimetric, and fluorescence methods (32). In comparison with the aforementioned methods, biosensors are favored because of their low cost, real-time monitoring capability and low equipment requirements. In this work, the LC properties of SS and COF supported SS ($COF_{TpBD-SS}$) were studied by resonance Rayleigh scattering (RRS) and Abs spectrophotometry. The $COF_{TpBD-SS}$ was prepared for the first time as a nanoparticle enzyme in the liquid phase in order to facilitate a catalytic Au nanoreaction. A novel PT biosensor with high sensitivity and selectivity was then constructed by combining the $COF_{TpBD-SS}$ with the PT biometric element to exploit the novel catalytic effect. Thereafter, a bi-mode biosensor platform was established, which afforded not only a SERS and Abs measurement capability but also was simple and of low-cost.

2. Experimental

2.1. Reagents and instrumentation

TU-1901 type dual-beam UV-Vis spectrophotometer (Beijing Puxi General Instrument Co., Ltd., Beijing, China); DXR Raman spectrometer (Thermo Fisher Scientific Company, Massachusetts, USA); Ultrasonic cleaner SK3300B (Shanghai

Kedao Ultrasonic Instrument Co., Ltd., Shanghai, China); SYZ-550 type quartz sub-boiling water distiller (Jiangsu Jingbo Instrument Factory, Jiangsu, China); DHG-9023A electric heating constant temperature blast drying oven (Shanghai Jinghong Experimental Equipment Co., Ltd., Shanghai, China); HH-1 electric heating constant temperature water bath (Shanghai Weicheng Instrument Co., Ltd., Shanghai, China); DF-101S-type heat-collecting constant temperature heating magnetic stirrer (Gongyi Yuhua Instrument Co., Ltd., Shanghai, China); High speed refrigerated centrifuge (GL-25MS, Shanghai Luxiangyi Centrifuge Instrument Co., Ltd., Shanghai, China).

Benzidine (BD, Jilin China Science and Technology Co., Ltd., Jilin, China); 2,5-dimethoxyterephaldehyde (DMTP, Shanghai Macklin Biochemical Co., Ltd., Shanghai, China); (SS, Xilong Science Co., Ltd., Santou, China); amylopectin (AP, Xilong Science Co., Ltd., Santou, China); dimethyl sulfoxide (DMSO, Xilong Chemical Co., Ltd., Santou, China); 2,4,6-trihydroxy-1,3,5-benzenetricarbaldehyde (Tp, Shanghai Macklin Biochemical Co., Ltd., Shanghai, China); acetone (AT, Xilong Science Co., Ltd., Santou, China); tetrahydrofuran (THF, Xilong Science Co., Ltd., Santou, China); Benzene-1,3,5-tricarbaldehyde (BTCA, Shanghai Macklin Biochemical Co., Ltd., Shanghai, China); 1,3,5-tris (4-aminophenyl)benzene (TAPB, Shanghai Macklin Biochemical Co., Ltd., Shanghai, China); 0.1% $HAuCl_4$ (1.0 mg/mL, National Group Chemical Reagent Co., Ltd., Shanghai, China); Peptide CW-Cd^{2+} (PT) sequence:Csy-Pro-Pro-Cys-Trp-NH_2 (Shanghai Apeptide Co., Ltd., Shanghai, China); 10^{-5}°mol/L Victoria Blue B (VBB) and 1 mol/L NaCl were used. The reagents used were of analytical grade, and the experimental water was sub-boiling distilled water.

2.2. Preparation of COF materials

2.2.1. Preparation of COF_{TpBD}

In a clean stoppered glass bottle (50 × 30), 6.5 mg of Tp (3 mmol/L), 20 mL of C_2H_5OH, and 2.5 mL of 3 mol/L acetic acid were added in succession. Dissolution of the reagents was achieved by agitation in an ultrasonic bath for 30 min. 8.3 mg of BD (4.5 mmol/L) was then added to the reaction mixture which was in an agitated state, and ultrasonic energy was applied again for 30 min. The reaction mixture was then washed with AT (3 × 10 mL) and THF (3 × 10 mL) successively and centrifuged at high speed (10,000 r/min, 10 min) to obtain a brown solid. The final product was freeze-dried for 21 h to obtain the brown COF_{TpBD} in powdered form.

2.2.2. Preparation of $COF_{TpBD-SS}$

Ten milliliter of 6.75 mmol/L BD solution, 10 mL of 4.5 mmol/L Tp solution and 10 mL of 3 mmol/L SS (the optimal conditions after optimization) were added to a clean corked glass bottle (50 × 30) while undergoing agitation for 30 min. A red-brown solid was obtained. Next, successive washings of the product with AT (3 × 10 mL) and THF (3 × 10 mL) were performed, and following high-speed low temperature centrifugation (10,000 r/min, 10 min), a yellow-brown solid was obtained. The final product was freeze-dried for 24 h, resulting in the $COF_{TpBD-SS}$ powder which was red-brown in color.

2.2.3. Preparation of $COF_{TpBD-AP}$

Ten milliliter of 6.75 mmol/L BD solution, 10 mL of 4.5 mmol/L Tp solution and 10 mL of 3 mmol/L AP (the optimal conditions after optimization) were added to a clean corked glass bottle (50 × 30) which was placed in an ultrasonic bath and agitated for 30 min. An orange-brown product was obtained. The product was washed with AT (3 × 10 mL) and THF (3 × 10 mL) in turn, and centrifuged at 10,000 r/min for 10 min to obtain an orange-brown solid. The final product was freeze-dried for 24 h to yield the $COF_{TpBD-AP}$ powder which was yellow-brown in color.

2.2.4. Preparation of COF_{TB}

19.6 mg of TAPB, 20 mL of DMSO and 1 mL of 3 mol/L HAc were added successively to a clean corked glass bottle (50 × 30) and the mixture was dissolved with the aid of ultrasonics for 30 min. Then, 10 mg of BTCA was added with mild stirring at room temperature, and the stirring continued for 1 min to obtain a yellow gel. The gel was next washed successively with AT (3 × 10 mL) and then THF (3 × 10 mL), and a dark yellow solid was obtained after high-speed and low temperature centrifugation (10,000 r/min, 10 min). The final product was freeze-dried for 21 h to yield the COF_{TB} powder which was yellow in color.

2.2.5. Preparation of COF_{BT-SS}

Ten milliliter of 8.4 mmol/L TAPB solution, 10 mL of 8.4 mmol/L BTCA solution and 8 mL of 3 mmol/L SS solution were successively in a clean corked glass bottle (50 × 30) which was agitated in an ultrasonic bath for 30 min. A yellow product was obtained and washed successively with AT (3 × 10 mL) and THF (3 × 10 mL), and a yellow solid was obtained after high-speed low temperature centrifugation (10,000 r/min, 10 min). The final product was freeze dried for 24 h to yield the COF_{BT-SS} which was a yellow powder.

2.2.6. Preparation of COF_{DT}

8.7 mg of DMTP, 20 mL of BA solution and 2.5 ml of 3 mol/L HAc were added successively to a clean corked glass bottle (50 × 30) and dissolved with the aid of ultrasonic agitation for 30 min. Then 10.5 mg of TAPB was added during stirring, and the stirring was continued for 2 h. Then the product was placed into an oven at 60 product h. The product was washed successively with AT (3 × 10 mL) and anhydrous THF (3 × 10 mL). A brown solid product was obtained after high-speed low temperature centrifugation (10,000 r/min, 10 min).

The final product was freeze-dried for 24 h to yield the brown COF_{DT} powder.

2.2.7. Preparation of COF_{DT-SS}

Ten milliliter of DMTP solution, 10 mL of TAPB solution, 2.5 mL of 3 mol/L acetic acid solution and 8.5 mL of 3 mmol/L SS solution (the optimal condition after optimization) were added to a clean corked glass bottle (50 × 30) during stirring for 2 h. The reaction mixture was then washed successively with AT (3 × 10 mL) and THF (3 × 10 mL), and a yellow-brown solid was obtained after high-speed low temperature centrifugation (10,000 r/min, 10 min). The final product was freeze-dried for 24 h to yield the COF_{DT-SS} which was a yellow-brown powder.

2.3. Experimental procedures

One hundred and seventy microliter of 0.1 mg/mL $COF_{TpBD-SS}$, 120 μL of 100 nmol/L PT, and various concentrations of $CdCl_2$ were added successively to a 5 mL calibrated tube, followed by 70 μL of 1 mg/mL $HAuCl_4$. Then 60 μL of 0.1 mol/L HCl followed by 120 μL of 0.1 mol/L Fo were then added; the mixture was shaken well and the volume made up to 2 mL. Next the solution was heated in a water bath at 80°C for 15 min. After the ice water was cooled to room temperature, 100 μL of 10^{-5} mol/L VBB and 100 μL of 1 mol/L NaCl were added. Then, the Raman spectrometer was used to record the SERS spectrum. The SERS intensity (I) at 1615 cm^{-1} was measured as was the SERS signal I_0 for the blank control solution (solution without Cd^{2+}) to allow the difference signal ($\Delta I = I–I_0$) to be calculated. In the case of spectrophotometric analysis, VBB was omitted and the absorbance (A) at 535 nm was measured. The absorbance of the blank solution A_0 (solution without Cd^{2+}) was also recorded. The difference in the absorbance values, $\Delta A = A\text{-}A_0$, was then calculated.

2.4. Sample preparation

Samples of rice grown in Hunan, Hubei, Guangxi and Wuchang were purchased from local stores. The rice samples were dried in an oven at 120°C for 8 h and ground with an agate mortar. Samples of 1.0 g (accurate to 0.1 mg) were transferred to 50 mL conical flasks containing 10 mL of mixed acid (vol $HN0_3$/vol $HClO_4$: 4:1) and left overnight (about 15 h). The samples were digested on a hot plate until white smoke appeared. When the solutions turned colorless and clear or slightly yellow, the samples were removed and left to cool before adjusting the volume to 10 mL. Finally, 100 μL aliquots of the digests were collected after filtration using a 0.45 μm microporous membrane filter.

3. Results and discussion

3.1. Principle of SERS/Abs bi-mode analysis

The COF material COF_{TpBD} was synthesized by stirring at room temperature using benzidine (Tp) and triuronic phloroglucinol (BD) as base reagents. Then SS was incorporated into the COF_{TpBD}, and SS was uniformly loaded on the surface of COF_{TpBD} *via* hydrogen bond interaction to enhance the catalytic effect of COF_{TpBD}. In general, in the absence of catalyst, Fo-$HAuCl_4$ reacted slowly and its SERS signal was low. $COF_{TpBD-SS}$ had a strong catalytic effect on the Fo-$HAuCl_4$ reaction, and the AuNPs exhibited a prominent SERS effect. Moreover, PT could be adsorbed on the surface of COF_{TpBD}, blocking contact between the active site and the reacting solution, thus inhibiting the catalytic effect. When Cd^{2+} was added to the solution, a stable conjugate was formed with PT, and COF_{TpBD} was released. The catalytic effect gradually recovered with increase of the Cd^{2+} concentration. The AuNPs generated gradually increased, and the AuNPs could be used as an active base for SERS. After adding the VBB probe molecules, the intensity of the SERS signal increased linearly as a function at 1,615 cm^{-1}. Meanwhile, the absorbance at 535 nm was enhanced with an increase in the content of the AuNPs. Based on the SERS and the Abs responses, the possibility of developing a highly selective and bi-mode spectrochemical (SERS/Abs) method for the determination of trace levels Cd^{2+} was conceived (**Figure 1**).

3.2. Material characterization

3.2.1. Electron microscopy

The COF and the nano catalytic amplification system were analyzed by transmission electron microscopy (TEM) and energy dispersive X-ray analysis (EDS). As shown in **Figure 2A**, COF_{TpBD} has a rod and layered type structure with particles of size about 450 nm; also, the diffraction peaks corresponding to C, N, and O occurred at 0.26, 0.40, and 0.53 keV, respectively (**Figure 2B**). In addition, as shown in **Figure 2C**, the COF_{TpBD} doped SS did not change its morphology. Given that $COF_{TpBD-SS}$ and COF_{TpBD} both contain elemental C, O, and N, it is not clear from the TEM and EDS spectra that SS is loaded on the surface of COF_{TpBD}. However, it is clear that the SS is indeed loaded on the surface of COF_{TpBD} based on inspection of the spectra of the variable temperature molecular, Raman and infrared spectroscopies. The TEM images of the AuNPs generated by the reaction of the PT-$COF_{TpBD-SS}$-AuNPs-Fo-$HAuCl_4$ (**Figures 2D, E**) showed that in the absence of Cd^{2+}, the AuNP were formed with an average particle size of 35 nm. In contrast, the addition of Cd^{2+} produced a large number of

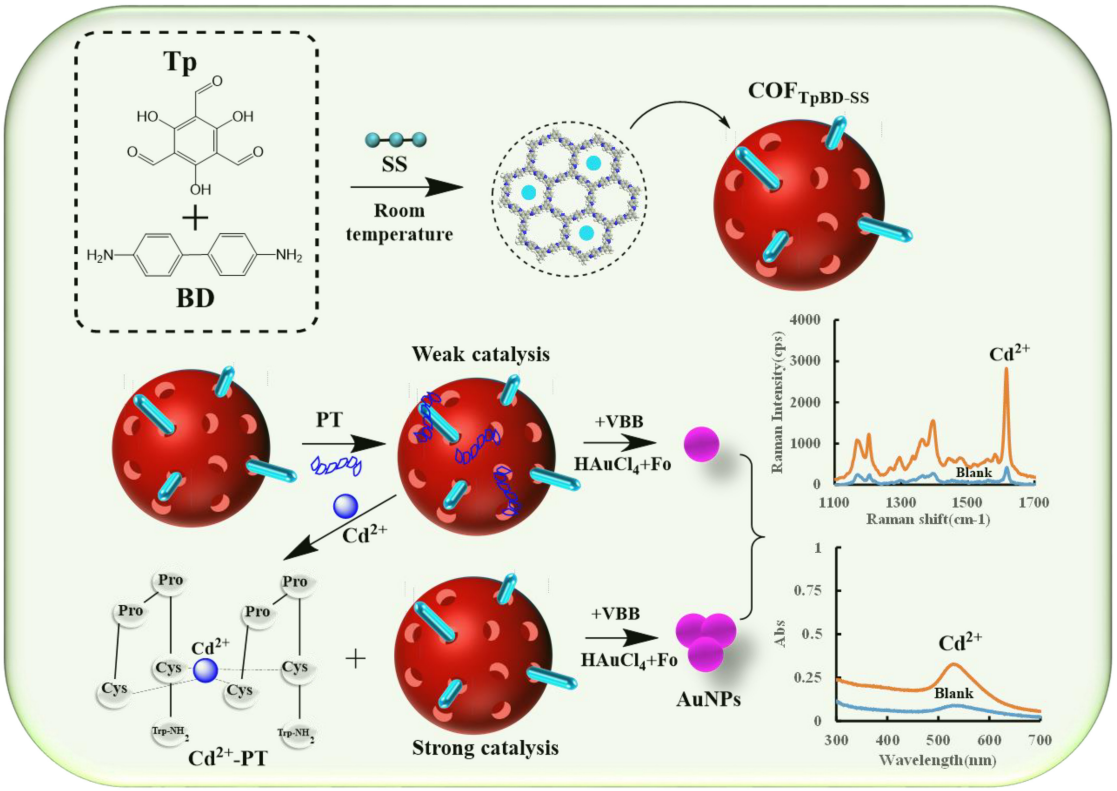

FIGURE 1
Schematic diagram of the SERS/Abs detection for Cd^{2+} coupled $COF_{TpBD-SS}$ catalysis amplification *via* PT.

AuNPs particles with an average particle size of about 55 nm, as evidenced by the spectral peak at 2.2 keV (**Figure 2F**).

3.2.2. Molecular spectra of nanomaterials

As shown in **Supplementary Figures 1A, B**, COF_{TpBD} had an absorption peak at 495 nm and SS had no absorption peak. After loading SS, the absorption peak of $COF_{TpBD-SS}$ had a slight red shift and appeared at 500 nm relative to COF_{TpBD} (**Supplementary Figure 1C**). It can be seen from consideration of the above that the spectral results of the two molecules are consistent. The absorption peaks of AP and $COF_{TpBD-AP}$ are shown in **Supplementary Figures 1D, E**. The UV variable temperature molecular absorption spectra of COF_{TpBD}, SS and $COF_{TpBD-SS}$ are presented in **Supplementary Figures 1F–H**. The Abs peak for COF_{TpBD} at 500 nm did not change with temperature, but the Abs peak for $COF_{TpBD-SS}$ at 500 nm occurred within the temperature range 70–950e temperatwas added to COF_{TpBD}. The absorbance increased with increase of temperature, but not before 70ea This indicated that $COF_{TpBD-SS}$ exhibited the characteristics of a thermotropic LC (33), reflecting the fact that SS confers LC properties, and that some of SS molecules may be exposed on the COF surface. In **Supplementary Figures 1I, J**, the Abs peaks of AP and $COF_{TpBD-AP}$ at 495 nm did not change with change in temperature indicating that AP and $COF_{TpBD-AP}$ did not exhibit the characteristics of a thermotropic LC.

RRS is a simple and sensitive technique for studying nanoparticles such as LCs, hence was used in this work. COF_{TpBD} and SS generate a characteristic RRS peak at 535 and 370 nm (**Figures 3A, B**), respectively. By examining the RRS spectrum of $COF_{TpBD-SS}$ (**Figure 3C**), it was found that after the loading of SS by COF_{TpBD}, the characteristic peak of COF_{TpBD} was observed at 535 nm, while the RRS peak for SS at 370 nm was not clear. The variable temperature RRS spectra of COF_{TpBD} and SS are shown in **Figures 3D, E**, respectively. The RRS peak of COF_{TpBD} at 545 nm did not change with change of temperature, while the RRS peak of SS at 370 nm was unchanged before 60°C, but did change within the temperature range 60–95°C, the intensity of the RRS peak increasing with increase of temperature. This demonstrated that SS has LC properties. By investigating the variable temperature RRS spectra of $COF_{TpBD-SS}$ (**Figure 3F**), it was found that after COF_{TpBD} was loaded with SS, two peaks appeared in the spectra, namely, at 300 and 535 nm. The two peaks did not change in appearance at temperatures less than 60°C. For temperatures between 60 and 95°C, the RRS intensity at 300 nm increased with increase in temperature (**Figures 3G, H**). The intensity of $COF_{TpBD-SS}$ was weaker than that of the SS. However,

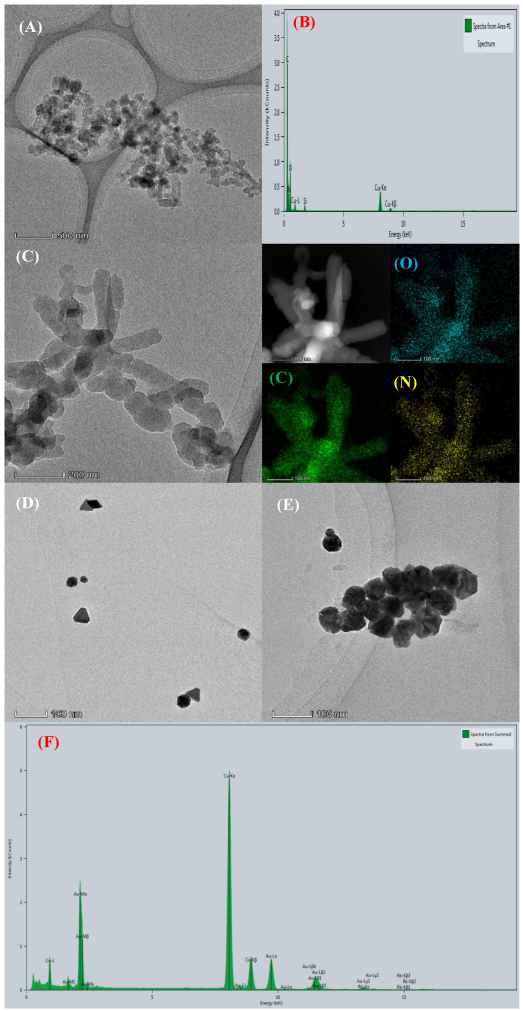

FIGURE 2
Transmission electron microscopy and energy dispersive X-ray analysis of the nanoparticles. **(A)** TEM of COF_{TpBD}; **(B)** EDS of COF_{TpBD}; **(C)** TEM of $COF_{TpBD-SS}$; **(D)** TEM of analysis system: 5 nmol/L PT + 2.5 mmol/L HCl + 6.25 μg/mL $COF_{TpBD-SS}$ + 0.025 mg/mL $HAuCl_4$ + 5 mmol/L Fo; **(E)** TEM of analysis system: D + 0.045 nmol/L Cd^{2+}; **(F)** EDS of analysis system.

the intensity of the $COF_{TpBD-SS}$ peak at 535 nm remained constant. The results would suggest that $COF_{TpBD-SS}$ had LC properties whereby some SS molecules were embedded into the COF porous structure, and some SS molecules may have been exposed on the COF surface. The variable temperature RRS spectra of AP and $COF_{TpBD-AP}$ are presented in **Figures 3I, J**. The RRS peak of $COF_{TpBD-AP}$ at 545 nm did not change with change of temperature, thus indicating that $COF_{TpBD-AP}$ did not exhibit the characteristics of thermotropic LCs.

The infrared spectrum of COF_{TpBD}/SS/$COF_{TpBD-SS}$ is shown in **Figure 3K**. Due to the introduction of SS, the electronic structure of the surface underwent modification, hence the FTIR spectrum did change. As shown in **Figure 3K**, COF_{TpBD} exhibited characteristic infra-red peaks near 2,436 cm^{-1}, which were attributed to the stretching vibration and in-plane rocking of the NH bond. The peaks for $COF_{TpBD-SS}$ were at 1,098 and 1,208 cm^{-1} relative to COF_{TpBD}. New peaks were formed, which were assigned to the C-O-C antisymmetric and symmetric stretching vibrations, indicating that the doping by SS may lead to changes in the surface structure of COF_{TpBD}. The structure of COF was confirmed by the Raman spectra for the COF_{TpBD} and $COF_{TpBD-SS}$ samples with AuNPs serving as the SERS substrate and NaCl as the aggregating agent (**Figure 3L**). COF_{TpBD} exhibited characteristic Raman peaks near 1,118, 1,187, 1,363, and 1,608 cm^{-1}, which were attributed to the torsional vibration, the in-plane rocking of the CH bond, the stretching vibration of the benzene ring and the C = C stretching vibration, respectively. Characteristic Raman peaks for $COF_{TpBD-SS}$ occurred at 1,195, 1,210, 1,413, and 1,625 cm^{-1}, and the peaks belonged to the in-plane rocking of the CH bond, the stretching vibration of the C-O-C, the stretching vibration of the benzene ring and the C = C stretching vibration, respectively. The SS has no clear characteristic peaks in the Raman spectrum. Compared with COF_{TpBD}, $COF_{TpBD-SS}$ had a "new" characteristic peak at 1,210 cm^{-1}, which was attributed to the stretching vibration of C-O-C. Due to the introduction of carbohydrate SS, the surface electronic structure had changed, hence the SERS spectrum changed. This indicated that a strong intermolecular force existed between the COF_{TpBD} and the SS, and the SS is well supported in the pores of COF_{TpBD}; this factor may well account for the enhanced catalytic activity.

3.2.3. Particle size distribution, surface charge analysis, and stability of $COF_{TpBD-SS}$

The particle size distribution of COF_{TpBD} was measured using a particle size analyzer. The particle sizes of most COF_{TpBD} particles ranged from 300 to 800 nm, and the average size was 522 nm. The average particle size of $COF_{TpBD-SS}$ was 1,412 nm after COF was loaded with SS, which reflects the incorporation of the long chain amylose (**Supplementary Figure 2A**). The charge distribution potentials for COF_{TpBD} and $COF_{TpBD-SS}$ were 0.0652 and 0.11 mV, respectively (**Supplementary Figures 2B, C**). The larger the absolute potential became, the more stable were the particles in the solution, and hence the stability of $COF_{TpBD-SS}$ was significantly improved (**Supplementary Figure 2C**).

To test the stability of COF_{TpBD}, SS and $COF_{TpBD-SS}$, changes in the charge distribution potential and their stability over time for solutions containing different concentrations of NaCl were studied, respectively. **Supplementary Figure 2D** shows that the absorbance values for COF_{TpBD} and SS and the mixed of SS and COF_{TpBD} solution decreased over time; the absorbance value for $COF_{TpBD-SS}$ was, however, stable, and the change was less than 5%. To study the stability of these catalytic materials in NaCl solutions of different concentrations, 150 μL

of 0.1 mg/mL COF_{TpBD}, SS and $COF_{TpBD-SS}$ were added into a series of 5 mL volumetric flasks. The absorbance signals were then measured by adding different volumes of 1 mol/L NaCl solution diluted with H_2O to 2 mL (**Supplementary Figure 2E**). The COF_{TpBD} and SS samples were found to be unstable in the different concentrations of NaCl solution, while the absorbance value for $COF_{TpBD-SS}$ was stable in low salinity solution. The absorbance value for the $COF_{TpBD-SS}$ solution decreased slightly with increasing NaCl concentration. The results showed that $COF_{TpBD-SS}$ was also stable in saline solution, while COF_{TpBD} and SS were relatively less stable. This was because SS could be evenly dispersed on the surface and in the pores of the COF_{TpBD} structure after COF_{TpBD} was loaded with SS, thus the stability of SS was greatly improved compared with that of COF_{TpBD} and SS.

3.2.4. X-ray diffraction (XRD) and specific surface area of COF_{TpBD}

Supplementary Figure 3A shows that COF_{TpBD} only has a diffraction peak near 25.7°, which corresponds to the (001) facet (34). Compared with COF_{TpBD}, $COF_{TpBD-SS}$ has no diffraction peaks of SS. This may be due to the low crystallinity of the loaded SS. To evaluate the permanent porosities and the surface area of COFs, the nitrogen adsorption-desorption isotherm was measured after degassing at 70°C for 6 h (**Supplementary Figure 3B**). According to the Brunauer–Emmett–Teller (BET) formula, the specific surface areas of COF_{TpBD} and $COF_{TpBD-SS}$ are calculated to be 256 and 1,033 $m^2\ g^{-1}$, respectively. The pore size distribution is illustrated in **Supplementary Figure 3C**, where the average pore sizes of COF_{TpBD} and $COF_{TpBD-SS}$ are 7.9 and 3.2 nm, respectively. The existence of the mesoporous structure can easily expose active sites and facilitate full contact with the reactants, effectively improving the catalytic efficiency.

3.3. SERS/Abs spectra of nano catalytic amplification system

Under experimental conditions, the AuNPs generated by the Cd^{2+}-PT-Fo-COF_{TpBD}/SS/$COF_{TpBD-SS}$/COF_{TB}/COF_{TB-SS}/COF_{DT}/COF_{DT-SS}-$HAuCl_4$ exhibited a strong SERS peak at 1,615 cm^{-1}. After adding PT to the catalytic system, due to the electrostatic effect, the PT would be adsorbed on the surface of the catalyst, resulting in a decrease in the catalytic activity and a reduction in the number of AuNPs generated, hence a decrease in the SERS signal occurred. When the unknown sample (test solution containing trace level of Cd^{2+}) was added to the inhibition system, PT was bound specifically to Cd^{2+} forming a stable structure, which detached from the catalyst surface. At the same time, the catalytic activity was restored, resulting in an increase in the number of the AuNPs generated by the nano system hence a recovery of the SERS signal (**Figure 4A**). Therefore, based on these SERS responses, it may be possible to establish a novel

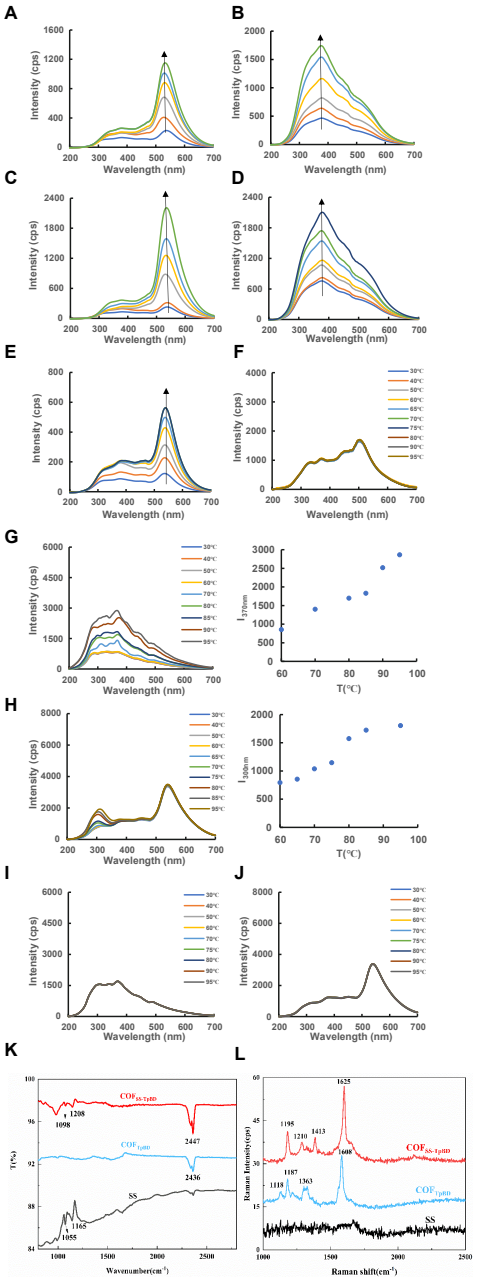

FIGURE 3
Resonance Rayleigh scattering spectra of COF_{TpBD}/SS/$COF_{TpBD-SS}$/AP/$COF_{TpBD-AP}$ and FTIR and SERS spectra of OF_{TpBD}/SS/$COF_{TpBD-SS}$. **(A)** COF_{TpBD} RRS spectra, 0.35, 1.25, 6.25, 12.5, 20, 25 μg/mL; **(B)** SS RRS spectra, 0.35, 2.5, 4.25, 12.5, 20, 25 μg/mL; **(C)** $COF_{TpBD-SS}$ RRS spectra 0.35, 0.7, 6.25, 12.5, 20, 25 μg/mL; **(D)** AP RRS spectra, 0.35, 1.25, 3.25, 6.25, 12.5, 20, 25 μg/mL; **(E)** $COF_{TpBD-AP}$ RRS spectra, 0.35, 3.25, 6.25, 12.5, 20, 25 μg/mL; **(F)** The RRS signal for 30 μg/mL of COF_{TpBD} with variation in temperature; **(G)** The RRS signal for 30 μg/mL of SS with variation in temperature; **(H)** The RRS signal for 30 μg/mL of $COF_{TpBD-SS}$ with variation in temperature; **(I)** The RRS signal for 30 μg/mL AP with variation in temperature; **(J)** The RRS signal for 30 μg/mL of $COF_{TpBD-AP}$ with variation in temperature; **(K)** the FTIR of COF_{TpBD}/SS/$COF_{TpBD-SS}$; **(L)** the SERS signal for 10 μg/mL of COF_{TpBD}/10 μg/mL SS/10 μg/mL $COF_{TpBD-SS}$ with 0.1 mmol/L AuNP + 0.05 mol/L NaCl + 0.5 μmol/L VBB.

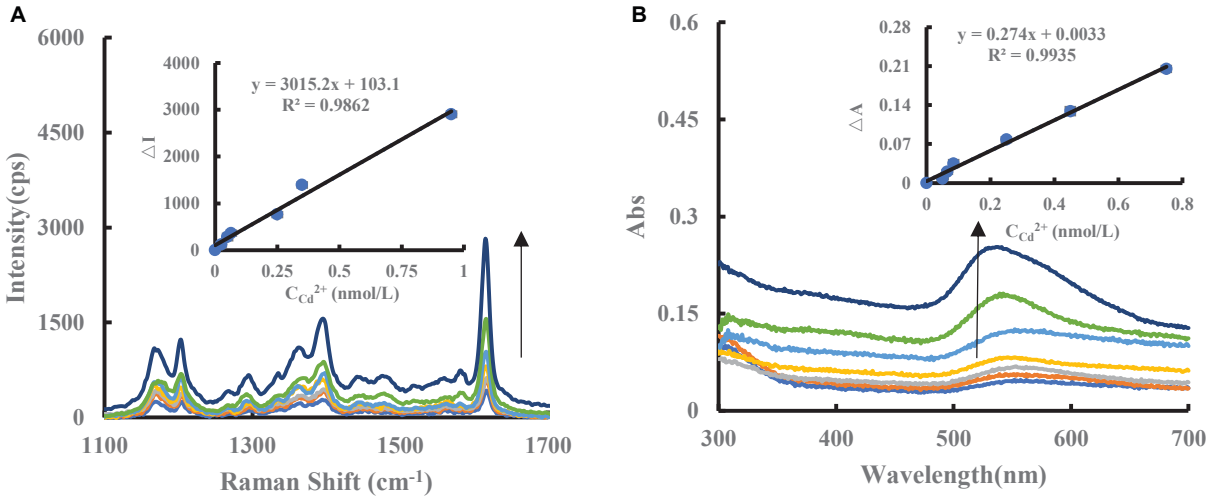

FIGURE 4
SERS/Abs spectra of catalytic amplification system. **(A)** (0, 0.025, 0.050, 0.065, 0.25, 0.35, 0.95) nmol/L Cd^{2+} + 5 nmol/L PT + 6.25 μg/mL $COF_{TpBD-SS}$ + 2.5 mmol/L Fo + 0.5 mmol/L HCl + 0.025 mg/mL $HAuCl_4$ + 0.5 μmol/L VBB + 0.05 mol/L NaCl; **(B)** Abs of (0, 0.05, 0.065, 0.085, 0.25, 0.45, 0.75) nmol/L Cd^{2+} + 5 nmol/L PT + 6.25 μg/mL $COF_{TpBD-SS}$ + 5 mmol/L Fo + 2.5 mmol/L HCl + 0.025 mg/mL $HAuCl_4$.

method for the measurement of Cd^{2+}. In addition, the SERS spectra of the COF_{TB}/COF_{TB-SS}/COF_{DT}/COF_{DT-SS}- $HAuCl_4$ system were recorded when different catalyst systems were used (**Supplementary Figures 4A–F**), however, as can be seen, the $COF_{TpBD-SS}$ system exhibited the largest slope. For the experimental conditions used, a surface plasmon resonance (SPR) absorption peak of Cd^{2+}-PT-$COF_{TpBD-SS}$-Fo-$HAuCl_4$ was observed at 535 nm (**Figure 4B**). This corresponded to the SPR absorption peak of the AuNPs.

3.4. Catalytic mechanism for $COF_{TpBD-SS}$

Regarding COF_{TpBD}, the particle size distribution observed was from 710 to 1990 nm for a solution of 6.25 μg/mL of $COF_{TpBD-SS}$ at 25°C. For a temperature of 80°C, the size distribution was from 100 to 340 nm. The average particle size of $COF_{TpBD-SS}$ was 286 nm. That is, an increase in temperature resulted in a smaller particle size, which correspondingly enhanced the catalytic activity of $COF_{TpBD-SS}$. Therefore, in the case of large size particles, the nanocatalytic reaction did not readily take place at room temperature, and hence cooling of the solution may be used to suppress or stop the nanocatalytic reaction. For the SS, the plot for the change of size with temperature was similar to that for $COF_{TpBD-SS}$ (**Supplementary Figure 5**).

Under the experimental conditions, the reaction of Fo and $HAuCl_4$ is slow, in which Au^{3+} is reduced to Au (I) and Au, and $HCOO^-$ is oxidized to CO_2. COF_{TpBD}/SS/$COF_{TpBD-SS}$/COF_{TB}/COF_{TB-SS}/COF_{DT}/COF_{DT-SS} catalyzes the $HAuCl_4$-Fo reaction (**Supplementary Table 1**). However, the AP and $COF_{TpBD-AP}$ did not exhibit catalytic activity. Regarding the slope of the linear equation in **Supplementary Table 1**, the slope of the $COF_{TpBD-SS}$ catalytic system is greater than the slope for the sum of COF_{TpBD} and SS, thus demonstrating an enhanced catalytic effect.

A low concentration of a SS solution has a relatively small particle size, hence the surface electrons can enhance the redox electron transfer in the $HAuCl_4$-Fo reaction (*cf* slope of 120.2). As is well known, SS is relatively unstable and can readily self-aggregate. When SS is loaded on the surface of COF_{TpBD}, its stability and the catalytic effect are greatly improved, and the slope of $COF_{TpBD-SS}$ is 303.9. Given that COF_{TpBD} has abundant pores and C = N bonds, there are a large number of π bonds and it is rich in π electrons, hence more active sites would be available for SS to be loaded on the surface, the size being limited by the pores. COF_{TpBD} acts as a carrier to make SS more evenly distributed and prevent its aggregation. When the particle size is at the nanometer scale, with increase in the number of surface atoms, the number of unsaturated bonds increase and the surface energy increases. The free electrons on the SS surface undergo coupling with the π electrons on the surface of COF_{TpBD}. The two sources of electrons greatly facilitate the transfer of electrons in the redox reaction of the $COF_{TpBD-SS}$–AuNPs, a process which is accelerated by the generation of AuNPs in the reaction hence the greatly enhanced catalytic activity (**Figure 5**). After PT is added to the nanosystem, due to the electrostatic effect, PT will be adsorbed on the surface of the catalyst and inhibit the catalytic activity. With increase in the PT concentration, the concentration of free catalyst in

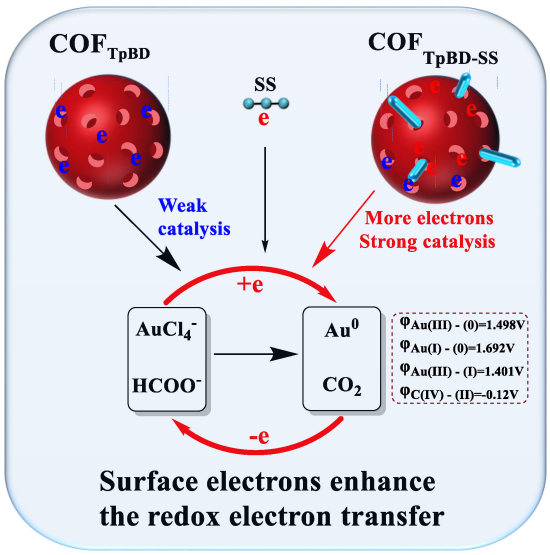

FIGURE 5
$COF_{TpBD-SS}$ nanocatalytic enhancement mechanism.

the system would decrease, and the catalytic activity would be weakened. Therefore, the AuNPs generated in the system would decrease as would the SERS signal (Supplementary Table 2), thus the inhibitory effect of PT was consistent with the observations of the catalytic effect. The main reactions are as follows:

$$Au(III) + Fo \xrightarrow{COF_{TpBD-SS}} Au(I) + CO_2 \quad (1)$$

$$Au(I) + Fo \xrightarrow{COF_{TpBD-SS}} Au + CO_2 \quad (2)$$

$$nAu = AuNPs \quad (3)$$

The relative standard electrode potential with common valence states of Au can be seen, E_0 (Au^{3+}/Au^0) = 1.498 V; E_0 (Au^+/Au^0) = 1.692 V; E_0 (Au^{3+}/Au^+) = 1.401 V. Therefore, due to the low redox potential of trivalent gold ion (Au^{3+}), it is difficult to reduce to gold nanoparticles (Au^0) in one step. As shown in Supplementary Figure 6, under the same conditions, Au^{3+} and Au^+ can be reduced by $HCOO^-$ to form Au^0. After the addition of $COF_{TpBD-SS}$ nanocomposite as catalyst, due to its large specific surface area and more active site, it can promote the reaction faster, accelerate the reduction of Au^{3+} into Au^+, and Au^+ into Au^0, and the reaction is easier to proceed.

3.5. Selection of conditions

3.5.1. Preparation conditions for $COF_{TpBD-SS}$

According to the experimental method, based on the strength of the catalytic effect of $COF_{TpBD-SS}$ nanosol on the Au-nanoindicator reaction, the corresponding conditions which yielded a strong catalytic effect were selected. The preparation conditions for the catalyst were optimized by changing the experimental conditions, respectively. When the loading condition for COF_{TpBD} with SS was 10 mL of 3 mmol/L (Supplementary Figure 7A), the amount of SS in COF_{TB} was 8 mL of 3 mmol/L (Supplementary Figure 7B), and the amount of SS in COF_{DT} was 8.5 mL of 3 mmol/L (Supplementary Figure 7C), then the ΔI of the catalytic system was maximized Therefore, these conditions were selected as the optimum experimental conditions.

3.5.2. Analysis conditions

The experimental conditions for SERS analysis were checked according to the experimental procedures. When the concentrations of the reactants/reagents were as follows: 6.25 μg/mL $COF_{TpBD-SS}$ (Supplementary Figure 8A), 5 nmol/L PT (Supplementary Figure 8B), 0.025 mg/mL $HAuCl_4$ (Supplementary Figure 8C), 2.5 mmol/L HCl (Supplementary Figure 8D), 5 mmol/L Fo (Supplementary Figure 8E), 0.5 μmol/L VBB (Supplementary Figure 8F), 0.05 mol/L NaCl (Supplementary Figure 8G), reaction temperature of 80°C Supplementary Figure 8H), reaction time of 15 min (Supplementary Figure 8I), the SERS response was optimal. The aforementioned conditions were chosen for SERS measurement.

3.6. Working (or analytical) curves

Using the optimized conditions, the corresponding ΔI/ΔA values for different concentrations of Cd^{2+} was plotted to obtain the working curve. It can be seen from Supplementary Tables 2, 3 that the slope of the working curve of the $COF_{TpBD-SS}$-Cd^{2+} system was 1 times that of COF_{TpBD} and 3 times that of SS, respectively, indicating that the former was the most sensitive (Figure 4A). The linear equation for spectrophotometric measurement was $\Delta I_{1,615\ cm^{-1}}$ = 3015.2C + 103.1, and the linear range was 0.025–0.95 nmol/L. Although the reaction time for the spectrophotometric method was relatively short, the sensitivity was less than SERS by a factor (Supplementary Table 3). Compared with the reported molecular spectroscopic methods for the determination of Cd^{2+} (35-37), the present SERS method is highly sensitive method (Supplementary Table 4).

3.7. Reproducibility and specificity

Reproducibility is an important indicator to be considered by biosensors, and it is only feasible with small coefficient

of variation (CV, also called relative standard deviation) (38). The intra-batch and inter-batch differences of SERS/Abs tests were conducted under 0.25 nmol/L cadmium standard solution (**Supplementary Figure 9**). In the same batch of tests, the Cd^{2+} was detected for 6 times. The results showed no difference, indicating that the intra-batch difference between individual biosensor tests was very small (**Supplementary Figure 9A**). In different 8 batches of tests, the Cd^{2+} was detected within the scope of effective detection (usually CV values $< 15\%$) at 0.25 nmol/L cadmium standard solution, suggesting that the inter-batch difference was within the acceptable range (**Supplementary Figure 9B**). The potential for interferences by coexisting ions on the SERS determination of 0.01 nmol/L Cd^{2+} was investigated. The experimental results indicated that in the presence of: (1) 1,000-fold excess of the following ions Mg^{2+}, Zn^{2+}, K^{+}, Al^{3+}, Na^{+}, Ca^{2+}, Ba^{2+}, Fe^{3+}, Mn^{2+}, Co^{2+}, Cu^{2+}, (2) 100-fold excess of Cr^{6+}, NH_4^{+}, Hg^{2+}, SO_4^{2-}, NO_2^{-}, I^{-}, and (3) 10-fold excess of CO_3^{2-}, PO_4^{3-}, Br^{-}, the aforementioned ions at the specified concentrations did not interfere with the measurement (**Supplementary Table 5**). Moreover, the relative error was within $\pm$ 10% hence the method afforded good selectivity for the determination of trace amounts of Cd^{2+}.

3.8. Determination of cadmium in rice

After sample pretreatment, in order to perform a recovery test, aliquots of standard solutions of Cd^{2+} were added to the digests. The Cd^{2+} content was determined according to the 2.3 experimental procedures. The analytical results are shown in **Supplementary Table 6**. The Cd^{2+} contents of the digests ranged from 0 to 0.31 nmol/L, which corresponded to Cd^{2+} contents in rice of 0–12.21 ng/g. The relative standard deviations (RSDs) ranged from 1.9 to 9.7%, and the recoveries were 91.2–109.7%, confirming that the SERS assay was accurate and reliable.

4. Conclusion

Based on loading SS nanoparticles into COFs, a novel $COF_{TpBD-SS}$ nanomaterial has been prepared. The nanomaterial not only enhanced catalytic activity but also had good stability. A nanoAu indicator reaction for $COF_{TpBD-SS}$ catalysis was investigated by molecular spectroscopy such that a SERS/Abs bi-mode method was developed for the determination of Cd^{2+} in rice based on exploiting the highly sensitive nanocatalytic amplification reaction based on the highly selective reaction with PT. The SERS analysis method was sensitive, whereas the Abs was relatively simple and of low cost. A plausible nanocatalytic mechanism was proposed whereby the nanosurface electrons enhanced the redox electron transfer to speed up the AuNP reaction.

Data availability statement

The original contributions presented in this study are included in the article/**Supplementary material**, further inquiries can be directed to the corresponding authors.

Author contributions

JL and YS: software, visualization, writing—original draft, investigation, and formal analysis. CL and ZJ: software, visualization, conception, reviewing and editing, software, methodology, validation, formal analysis, and supervision. All authors contributed to the article and approved the submitted version.

Funding

This work was supported by the Scientific Research Foundation of Guangxi Education Department (no. 2022KY0509), the National Natural Science Foundation of China (nos. 22266013 and 22264005), and the Natural Science Foundation of Guangxi (no. 2022GXNSFDA035073).

Conflict of interest

The authors declare that the research was conducted in the absence of any commercial or financial relationships that could be construed as a potential conflict of interest.

Publisher's note

Supplementary material

The Supplementary Material for this article can be found online at: https://www.frontiersin.org/articles/10.3389/fnut.2022.1075296/full#supplementary-material

References

1. Mehta, P, Neupane L, Park S, Lee K. Ratiometric fluorescent detection of silver nanoparticles in aqueous samples using peptide-based fluorogenic probes with aggregation-induced emission characteristics. *J Hazard Mater.* (2021) 411:125041. doi: 10.1016/j.jhazmat.2021.125041

2. Zhi S, Wei Q, Zhang C, Yi C, Li C, Jiang Z. MXene catalytic amplification-fluorescence/absorption dimode aptamer sensor for the detection of trace Pb^{2+} in milk. *Front Nutr.* (2022) 9:1008620. doi: 10.3389/fnut.2022.1008620

3. Zhuang H, Jiang X, Wu S, Wang S, Pang Y, Huang Y, et al. A novel polypeptide-modified fluorescent gold nanoclusters for copper ion detection. *Sci Rep.* (2022) 12:6624. doi: 10.1038/s41598-022-10500-9

4. Yu B, Cui Y, Mao X, Li Z, Li Z, Shi G. A time-resolved fluorescence lateral flow immunochromatographic assay based on oriented immobilized antibodies for the ultrasensitive detection of C-peptides in human serum. *Anal Chim Acta.* (2022) 1208:339833. doi: 10.1016/j.aca.2022.339833

5. Damayanti N, Buno K, Voytik Harbin S, Irudayaraj J. Epigenetic process monitoring in live cultures with peptide biosensors. *ACS Sens.* (2019) 4:562–5. doi: 10.1021/acssensors.8b01134

6. Islam S, Powner M. Prebiotic systems chemistry: complexity overcoming clutter. *Chem.* (2017) 2:470–501. doi: 10.1016/j.chempr.2017.03.001

7. Foden C, Islam S, Fernández-García C, Maugeri L, Sheppard T, Powner M. Prebiotic synthesis of cysteine peptides that catalyze peptide ligation in neutral water. *Science.* (2020) 370:865–9. doi: 10.1126/science.abd5680

8. Samoylenko A, Kögler M, Zhyvolozhnyi A, Makieieva O, Bart G, Andoh S, et al. Time-gated Raman spectroscopy and proteomics analyses of hypoxic and normoxic renal carcinoma extracellular vesicles. *Sci Rep.* (2021) 11:19594. doi: 10.1038/s41598-021-99004-6

9. Kuramochi H, Takeuchi S, Kamikubo H, Kataoka M, Tahara T. Fifth-order time-domain Raman spectroscopy of photoactive yellow protein for visualizing vibrational coupling in its excited state. *Sci Adv.* (2019) 5:eaau4490. doi: 10.1126/sciadv.aau4490

10. Fang W, Jia S, Chao J, Wang L, Duan X, Liu H, et al. Quantizing single-molecule surface-enhanced Raman scattering with DNA origami metamolecules. *Sci Adv.* (2019) 5:eaau4506. doi: 10.1126/sciadv.aau4506

11. Qu G, Zhang G, Wu Z, Shen A, Wang J, Hu JA. "turn-off" SERS assay of heparin with high selectivity based on heparin–peptide complex and Raman labelled gold nanoparticles. *Biosens Bioelectron.* (2014) 60:124–9. doi: 10.1016/j.bios.2014.04.004

12. Liang A, Li C, Li D, Luo Y, Wen G, Jiang Z. A facile and sensitive peptide-modulating graphene oxide nanoribbon catalytic nanoplasmon analytical platform for human chorionic gonadotropin. *Int J Nanomedicine.* (2017) 12:8725–34. doi: 10.2147/IJN.S149536

13. Lan Y, Han X, Tong M, Huang H, Yang Q, Liu D, et al. Materials genomics methods for high-throughput construction of COFs and targeted synthesis. *Nat Commun.* (2018) 9:5274. doi: 10.1038/s41467-018-07720-x

14. Yuan S, Li X, Zhu J, Zhang G, Van Puyvelde P, Van der Bruggen B. Covalent organic frameworks for membrane separation. *Chem Soc Rev.* (2019) 48:2665–81. doi: 10.1039/C8CS00919H

15. Lohse M, Bein T. Covalent organic frameworks: structures, synthesis, and applications. *Adv Funct Mater.* (2018) 28:1705553. doi: 10.1002/adfm.201705553

16. Liu Y, Wu H, Wu S, Song S, Guo Z, Ren Y, et al. Multifunctional covalent organic framework (COF)-Based mixed matrix membranes for enhanced CO_2 separation. *J Membr Sci.* (2021) 618:118693. doi: 10.1016/j.memsci.2020.118693

17. Lyle S, Waller P, Yaghi O. Covalent organic frameworks: organic chemistry extended into two and three dimensions. *Trends Chem.* (2019) 1:172–84. doi: 10.1016/j.trechm.2019.03.001

18. Wang H, Zhao Y, Shi J, Wen G, Liang A, Jiang Z. A novel aptamer RRS assay platform for ultratrace melamine based on COF-loaded Pd nanocluster catalytic amplification. *J Hazard Mater.* (2022) 423:127263. doi: 10.1016/j.jhazmat.2021.127263

19. Geng K, He T, Liu R, Dalapati S, Tan K, Li Z, et al. Covalent organic frameworks: design, synthesis, and functions. *Chem Rev.* (2020) 120:8814–933. doi: 10.1021/acs.chemrev.9b00550

20. Lei Z, Yang Q, Xu Y, Guo S, Sun W, Liu H, et al. Boosting lithium storage in covalent organic framework via activation of 14-electron redox chemistry. *Nat Commun.* (2018) 9:576. doi: 10.1038/s41467-018-02889-7

21. He J, Xu F, Chen Z, Hou X, Liu Q, Long Z. AuNPs/COFs as a new type of SERS substrate for sensitive recognition of polyaromatic hydrocarbons. *Chem Commun.* (2017) 53:11044–7. doi: 10.1039/C7CC06440C

22. Shu Y, Zhi S, Li S, Liang A, Jiang Z. A new peptide-mediated COF nanocatalytic amplification SERS quantitative assay for ultratrace Cu^{2+}. *J Ind Eng Chem.* (2022) 113:196–205. doi: 10.1016/j.jiec.2022.05.046

23. Yao D, Li C, Wang H, Wen G, Liang A, Jiang Z. A new dual-mode SERS and RRS aptasensor for detecting trace organic molecules based on gold nanocluster-doped covalent-organic framework catalyst. *Sens Actuators B Chem.* (2020) 319:128308. doi: 10.1016/j.snb.2020.128308

24. Wang H, Bai H, Wen G, Liang A, Jiang Z. Efficient nanocatalytic amplification of COF-loaded liquid crystal coupling with free-label aptamer to determine trace small molecular drugs by SERS quantitative strategy. *Appl Mater Today.* (2022) 27:101490. doi: 10.1016/j.apmt.2022.101490

25. Zugenmaier P, Voihsel M. A new class of polymeric liquid crystals: lyotropic amylose ethers. *Makromol Chem Rapid Commun.* (1984) 5:245–53. doi: 10.1002/marc.1984.030050502

26. Oyamada K, Terao K, Suwa M, Kitamura S, Sato T. Lyotropic liquid crystallinity of amylose tris(alkylcarbamates): cholesteric and smectic phase formation in different solvents. *Macromolecules.* (2013) 46:4589–95. doi: 10.1021/ma400787c

27. Balasurya S, Syed A, Swedha M, Harini G, Elgorban A, Zaghloul N, et al. A novel SPR based Fe@Ag core–shell nanosphere entrapped on starch matrix an optical probe for sensing of mercury(II) ion: a nanomolar detection, wide pH range and real water sample application. *Spectrochim Acta A Mol Biomol Spectrosc.* (2021) 263:120204. doi: 10.1016/j.saa.2021.120204

28. Sapyen W, Toonchue S, Praphairaksit N, Imyim A. Selective colorimetric detection of Cr(VI) using starch-stabilized silver nanoparticles and application for chromium speciation. *Spectrochim Acta A Mol Biomol Spectrosc.* (2022) 274:121094. doi: 10.1016/j.saa.2022.121094

29. Chen G, Shah K, Shi L, Chiang P. Removal of Cd(II) and Pb(II) ions from aqueous solutions by synthetic mineral adsorbent: performance and mechanisms. *Appl Surf Sci.* (2017) 409:296–305. doi: 10.1016/j.apsusc.2017.03.022

30. Hua Y, Zheng X, Xue L, Han L, He S, Mishra T, et al. Microbial aging of hydrochar as a way to increase cadmium ion adsorption capacity: process and mechanism. *Bioresour Technol.* (2020) 300:122708. doi: 10.1016/j.biortech.2019.122708

31. Elkady M, Abu-Saied M, Abdel Rahman A, Soliman E, Elzatahry A, Elsayed Yossef M, et al. Nano-sulphonated poly (glycidyl methacrylate) cations exchanger for cadmium ions removal: effects of operating parameters. *Desalination.* (2011) 279:152–62. doi: 10.1016/j.desal.2011.06.002

32. Behbahani E, Dashtian K, Ghaedi M. Fe_3O_4-$FeMoS_4$: promise magnetite LDH-based adsorbent for simultaneous removal of Pb (II), Cd (II), and Cu (II) heavy metal ions. *J Hazard Mater.* (2021) 410:124560. doi: 10.1016/j.jhazmat.2020.124560

33. Huang H, Li J, Pan S, Wang H, Liang A, Jiang Z. A novel small molecular liquid crystal catalytic amplification-nanogold SPR aptamer absorption assay for trace oxytetracycline. *Talanta.* (2021) 233:122528. doi: 10.1016/j.talanta.2021.122528

34. Chen X, Addicoat M, Jin E, Xu H, Hayashi T, Xu F, et al. Designed synthesis of double-stage two-dimensional covalent organic frameworks. *Sci Rep.* (2015) 5:14650–69. doi: 10.1038/srep14650

35. Wang P, Wu J, Zhao C. A water-soluble peptide fluorescent chemosensor for detection of cadmium (II) and copper (II) by two different response modes and its application in living LNcap cells. *Spectrochim Acta A Mol Biomol Spectrosc.* (2020) 226:117600. doi: 10.1016/j.saa.2019.117600

36. Serrano N, Prieto-Simón B, Cetó X, del Valle M. Array of peptide-modified electrodes for the simultaneous determination of Pb(II), Cd(II) and Zn(II). *Talanta.* (2014) 125:159–66. doi: 10.1016/j.talanta.2014.02.052

37. Jiang X, Xia J, Luo X. Simple, rapid, and highly sensitive colorimetric sensor strips from a porous cellulose membrane stained with Victoria blue B for efficient detection of trace Cd(II) in water. *ACS Sustain Chem Eng.* (2020) 8:5184–91. doi: 10.1021/acssuschemeng.9b07614

38. Wu Z, Lu J, Fu Q, Sheng L, Liu B, Wang C, et al. A smartphone-based enzyme-linked immunochromatographic sensor for rapid quantitative detection of carcinoembryonic antigen. *Sens Actuators B Chem.* (2021) 329:129163. doi: 10.1016/j.snb.2020.129163